Progress In Electromagnetics Research C, Vol. 172, 103–114, 2026
PIER C

(Received 6 May 2026, Accepted 8 June 2026, Scheduled 1 August 2026)

Improved Full-Order Model-Free Sliding Mode Control for PMSM Considering Complex Time-Varying Disturbances

Xingkai Huang, Xiangfei Li*, Kaihui Zhao, Meiyun Luo, and Lihua Zou

School of Transportation and Electrical Engineering, Hunan University of Technology, China

ABSTRACT: To address the problems of low speed control accuracy and performance degradation caused by time-varying disturbances in conventional control methods for high-precision speed regulation of permanent magnet synchronous motors (PMSMs), an improved full-order model-free sliding mode control (IFOMFSMC) method based on full-order sliding mode control (FOSMC) is proposed. First, a novel ultra-local model under parameter perturbations is established. Based on this model, the IFOMFSMC is designed by combining a second-order full-order sliding mode surface with an improved double-power reaching law, which improves the speed control accuracy of the PMSM. Subsequently, a full-order extended sliding mode disturbance observer (FOESMDO) is developed by incorporating FOSMC into the extended disturbance observer. The FOESMDO estimates unknown disturbances more accurately, thereby compensating the IFOMFSMC and enhancing system robustness under complex time-varying disturbances. Finally, simulation results confirm accurate speed tracking with the proposed method. Under complex time-varying disturbance conditions, compared with the conventional control method, the IFOMFSMC improves speed response and tracking performance by 57.6% and 88.2%, respectively, while reducing steady-state speed error and torque ripple by 71.8% and 29.2%. The proposed method effectively enhances steady-state and dynamic performance as well as disturbance-rejection capability.

1. INTRODUCTION

Permanent magnet synchronous motors (PMSMs) are extensively used in various industrial sectors, including high-speed trains and electric vehicles, owing to their high power density and compact size [1]. Achieving high-precision speed regulation of PMSM is not only an urgent requirement for promoting industrial upgrading but also a strategic key to seizing the commanding heights of high-end equipment. However, the dominant conventional proportional-integral (PI) control often suffers from performance degradation in practical systems due to uncertain factors, such as parameter perturbations, unmodeled dynamics, and external disturbances, making it difficult to meet PMSM control requirements in demanding applications [2].

In recent years, to achieve high-performance control of PMSM, advanced control approaches, such as sliding mode control [3], neural network control [4], and adaptive control [5], have been widely adopted, yielding significant performance improvements. However, these methods are strongly dependent on an accurate mathematical model and nominal motor parameters, and their robustness is limited under time-varying parameters and strong coupling conditions. Model-free control (MFC), which designs a controller using only system input-output data, offers a new approach to solving the model dependence problem.

Owing to its simple algorithm and strong robustness against external disturbances, sliding mode control (SMC) has been widely used in disturbance observation and motor control [6, 7]. For this reason, Zhao et al. [8] combined SMC with MFC to design a model-free sliding mode controller (MFSMC) and employ a sliding mode observer to estimate unknown disturbances, thereby solving the model dependence problem and improving system robustness. Based on this, Zhao et al. [9] established a new ultra-local model, improved the feedback controller of the speed loop, and proposed an extended sliding mode disturbance observer (ESMDO), further enhancing the system's disturbance-rejection capability. Based on [9], Li et al. [10] introduced a second-order non-singular fast terminal sliding mode surface to accelerate error convergence and suppress chattering. In [11], a third-order super-twisting algorithm is applied to both the feedback controller and the disturbance observer, further improving the convergence rate and disturbance-rejection capability. The works in [10] and [11] improved the convergence rate of the rotational speed and reduced the steady-state speed error by refining the sliding mode surface and the reaching law. However, this type of improvement belongs to a control method that performs differentiation and order reduction on the sliding mode surface. For PMSM's high-precision control, such reduced-order methods face the limitation that the actual speed cannot reach the reference speed. Once in steady state, any deviation of the actual speed from the reference speed causes the switching control law to cease switching and the output to remain constant, thereby rendering the switching control function ineffective. This problem causes reduced-order MFSMC to fail to meet precision requirements of high-accuracy PMSM speed regulation applications. Therefore, incorporating a new control strategy into the conventional MFSMC is required to solve this problem.

* Corresponding author: Xiangfei Li (lixiangfei2006@163.com).

Full-order sliding mode control (FOSMC) eliminates the reduced-order design, does not require direct differentiation of the sliding mode surface, and can generate a continuous control law. As a result, chattering is strongly suppressed, and the system exhibits the desired full-order dynamic characteristics [12]. In [13], FOSMC was combined with a super-twisting algorithm to design an observer for a two-link manipulator system. This approach achieved accurate estimation of the derivatives of the system states and reduced the difficulty of controller design. In [14], a high-performance controller was designed combining FOSMC with the bilimit homogeneous property, achieving fixed-time convergence and chattering suppression for a servo motor system. In [15], FOSMC is adopted for the current control of a permanent magnet synchronous generator, which mitigates chattering in the system and significantly improves current tracking accuracy. Although the aforementioned studies have improved system control performance by introducing FOSMC, the existing FOSMC design still heavily depends on the system's mathematical model, and its control performance becomes unsatisfactory under time-varying parameters and complex disturbances in PMSM.

To address the above problems, this paper proposes an improved full-order model-free sliding mode control (IFOMFSMC) method based on FOSMC. This method achieves high-precision speed control of PMSM, solves the model dependence problem, and effectively enhances the dynamic and steady-state performance as well as the disturbance-rejection capability of the control system under complex time-varying disturbances compared with conventional control methods.

The main contributions of this study are as follows:

(i) By combining FOSMC with MFSMC, a full-order model-free sliding mode control (FOMFSMC) method was designed, which reduces dependence on model parameters while achieving high-precision speed control of PMSM.

(ii) The FOMFSMC was improved, and the IFOMFSMC was developed. By introducing a new term to design the second-order full-order sliding mode surface, the controller output as a whole cleverly becomes an integral term. The controller was precisely limited by the intersection value of the maximum torque per ampere (MTPA) curve and current-limit circle, which reduces the steady-state error of rotational speed and greatly decreases the overshoot occurring in the FOMFSMC. Subsequently, the sliding mode surface was combined with the improved double-power reaching law to enhance the system's response speed.

(iii) The FOSMC was introduced into an ESMDO to design a full-order extended sliding mode disturbance observer (FOESMDO), which estimates disturbances more accurately to compensate the controller, thereby enhancing the disturbance rejection capability and the system's control precision.

The remainder of this paper is organized as follows. Section 2 establishes the mathematical model of PMSM considering time-varying disturbances. Section 3 presents an FOMFSMC based on an ESMDO. Section 4 presents an IFOMFSMC based on an FOESMDO. Section 5 presents the simulation results. Finally, Section 6 concludes the study.

2. MATHEMATICAL MODEL OF PMSM

Under assumptions of no magnetic saturation and negligible core losses, the following voltage equations are obtained in the rotor reference frame [16]:

$$\begin{cases} u_d = R_s i_d + L_d \frac{\mathrm{d}i_d}{\mathrm{d}t} - \omega_e L_q i_q \\ u_q = R_s i_q + L_q \frac{\mathrm{d}i_q}{\mathrm{d}t} + \omega_e (L_d i_d + \psi_f) \end{cases} \tag{1}$$

where i_d, i_q and u_d, u_q are the d-q axis stator currents and voltages; L_d, L_q are the d-q axis inductances; ψ_f is the permanent magnet flux linkage; R_s is the stator resistance; and ω_e is the electrical angular velocity.

Taking into account electromagnetic parameter perturbations, the PMSM stator voltage equations are expressed as

$$\begin{cases} u_d = R_s i_d + L_d \frac{\mathrm{d}i_d}{\mathrm{d}t} - \omega_e L_q i_q + \Delta u_d \\ u_q = R_s i_q + L_q \frac{\mathrm{d}i_q}{\mathrm{d}t} + \omega_e (L_d i_d + \psi_\mathrm{f}) + \Delta u_q \end{cases} \tag{2}$$

where Δu_d and Δu_q denote the disturbance voltages on the d-q axis caused by parametric uncertainties in R_s, L_d, L_q, and ψ_f.

$$\begin{cases} \Delta u_d = \Delta R_s i_d + \Delta L_d \frac{\mathrm{d}i_d}{\mathrm{d}t} - \omega_e \Delta L_q i_q \\ \Delta u_q = \Delta R_s i_q + \Delta L_q \frac{\mathrm{d}i_q}{\mathrm{d}t} + \omega_e (\Delta L_d i_d + \Delta\psi_\mathrm{f}) \end{cases} \tag{3}$$

The PMSM electromagnetic torque equation is presented as

$$\begin{aligned} T_e &= \frac{3}{2} n_p [\psi_f + (L_d - L_q) i_d] i_q + \Delta T_e \\ &= \frac{3}{2} n_p \psi_{ext} i_q + \Delta T_e \end{aligned} \tag{4}$$

where T_e denotes the electromagnetic torque of the PMSM; n_p gives the pole pair count; $\Delta T_e = \frac{3}{2} n_p [\psi_r + (\Delta L_d - \Delta L_q) i_d] i_q$ represents the perturbation of the electromagnetic torque; and $\psi_{ext} = \psi_f + (L_d - L_q) i_d$ corresponds to the effective flux linkage.

The equation of the PMSM is given as follows for the mechanical motion:

$$\frac{\mathrm{d}\omega_e}{\mathrm{d}t} = \frac{n_p}{J}(T_e - T_L - B_m \omega_m) + \Delta P_n \tag{5}$$

where ω_m, T_L, B_m, J, and ΔP_n denote the mechanical angular velocity, load torque, viscous friction coefficient, rotational inertia, and perturbation of the mechanical parameter, respectively.

Substituting (4) into (5) yields an ultra-local model for the PMSM's speed loop [9].

$$\begin{aligned} \frac{\mathrm{d}\omega_e}{\mathrm{d}t} &= \frac{3 n_p^2}{2J} \psi_{ext} i_q - \frac{B}{J}\omega_e - \frac{n_p}{J}(\Delta T_e - T_L + \Delta T_L) \\ &= \gamma i_q + \xi \omega_e + F \end{aligned} \tag{6}$$

where the parameters to be designed are γ and ξ, given by $\gamma = 3n_p^2\psi_{ext}/2J$ and $\xi = -B/J$; F represents the total uncertain disturbance of the system.

Assumption 1 *The uncertainties of the motor parameters are known and satisfy (7).*

$$\Theta \in \Omega_\Theta \triangleq \{\Theta : \Theta_{\min} \leq \Theta \leq \Theta_{\max}\} \tag{7}$$

where $\Theta = [J\, R\, L_d\, L_q\, \psi_f\, B_m]^T$ *is the vector of controlled parameters in the speed loop equation;* $\Theta_{\min}$ *and* $\Theta_{\max}$ *denote the lower and upper bounds of* Θ*, respectively.*

Assumption 2 *The unknown time-varying disturbance is bounded and satisfies (8).*

$$|F| \leq F_{\max} < +\infty \tag{8}$$

where $F_{\max}$ *represents the upper bound of* F*, which can be obtained by estimation in practical engineering.*

3. DESIGN OF FOMFSMC BASED ON ESMDO

This section describes how the FOSMC is combined with the MFSMC to design the FOMFSMC. Furthermore, an ESMDO was developed to strengthen capability of the control system for disturbance rejection.

3.1. Background of the FOSMC

In conventional SMC, chattering is caused by the switching function, which degrades system stability and precision. To resolve this chattering problem, the FOSMC is adopted in this study. With the FOSMC, the system can achieve ideal full-order dynamics throughout sliding mode motion. Additionally, because the control law removes the term with a negative exponent associated with the system state, singularities in the control system are avoided.

Consider the nonlinear high-order system described by (9):

$$\begin{cases} \dot{x}_1 = x_2 \\ \dot{x}_2 = x_3 \\ \cdots \\ \dot{x}_n = a(x,t) + b(x,t) + c(x,t)u \end{cases} \tag{9}$$

where the state vector of the system is x; n is the order of the system; $|b(x,t)| \leq D$ denotes the external disturbance; $a(x,t)$ and $c(x,t)$ are linear functions; and u is the control input to be designed.

For the sliding mode function s, the design adopted in (10) is [12]:

$$s = \dot{x}_n + c_n \operatorname{sgn}(x_n)|x_n|^{\mu_n} + \cdots + c_1 \operatorname{sgn}(x_1)|x_1|^{\mu_1} \tag{10}$$

where c_i $(i = 1, \ldots, n)$ and μ_i $(i = 1, \ldots, n)$ are coefficients, with n denoting the order of the nonlinear system. The coefficients c_i are chosen such that the polynomial $p^n + c_n p^{n-1} + \cdots + c_2 p + c_1$ satisfies the Hurwitz stability condition, which implies that every eigenvalue of the polynomial lies strictly in the left half of the complex plane. Meanwhile, parameter μ_i is determined by the following (11):

$$\begin{cases} \mu_i = \mu, \ \ i = 1 \\ \mu_{i-1} = \frac{\mu_i \mu_{i+1}}{2\mu_{i+1} - \mu_i} \, (i = 2, \ldots, n) \ \ n \geq 2 \end{cases} \tag{11}$$

where $\mu_{i+1} = 1$, $\mu_i = \mu$, $\mu \in (1-\theta, 1)$ and $\theta \in (0, 1)$.

To ensure that system (9) reaches a steady state in a finite time, the following control law is designed:

$$u = c^{-1}(x,t)\,(u_{eq} + u_{st}) \tag{12}$$

The equivalent control law u_{eq} is expressed as:

$$\begin{aligned} u_{eq} \ &= \ -a(x,t) - c_n \operatorname{sgn}(x_n)|x_n|^{\mu_n} - \cdots - \\ &\quad c_1 \operatorname{sgn}(x_1)|x_1|^{\mu_1} \end{aligned} \tag{13}$$

The switching control law u_{st} is expressed as [12]:

$$\dot{u}_{st} + Tu_{st} = v \tag{14}$$

$$v = -(k_D + k_{TD} + \sigma)\operatorname{sgn}(s) \tag{15}$$

where k_D is the parameter chosen that exceeds the upper bound of the derivative of the external disturbance, that is, the derivative of the external disturbance in absolute value and the control gains must satisfy $k_D \geq |b(x,t)|$, $k_{TD} \geq T$ and $\sigma > 0$.

From (14) and (15), the FOSMC's switching control law is expressed by a differential equation. Solving this yields a general solution of exponential form for the switching control law, and the system remains continuous. Accordingly, the switching term of this control law can be sufficiently large to drive the system into the sliding mode rapidly, and no chattering occurs in the controller.

Taking the Laplace transform of (14) yields the following form [15]:

$$\frac{u_{st}(s)}{v(s)} = \frac{1}{s+T} \tag{16}$$

Therefore, (14) effectively acts as a low-pass filter. By attenuating the high-frequency components of the input signal, the dynamic response is successfully smoothed, and in turn, chattering is suppressed to a great extent.

3.2. Design of FOMFSMC

The FOSMC was introduced into the MFSMC and combined with the exponential reaching law to design the FOMFSMC. According to (6), the control law for PMSM speed control is designed as (17) [9]:

$$i_q^* = \frac{\dot{\omega}_e^* - \xi\omega_e - F + u_c}{\gamma} \tag{17}$$

where i_q^* is the current component of the q axis given by the control system; ω_e^* is the speed given to the system; and u_c is the output from the FOMFSMC controller.

Substituting (17) into (6) yields:

$$u_{c1} = -(\dot{\omega}_e^* - \dot{\omega}_e) \tag{18}$$

The speed controller state error e is defined as:

$$e = \omega_e^* - \omega_e \tag{19}$$

The speed error is selected as the state variable of the controller:

$$x_1 = e = \omega_e^* - \omega_e \tag{20}$$

Differentiating x_1 in (20) and substituting (18) yields

$$\dot{x}_1 = -u_{c1} = \dot{\omega}_e^* - \dot{\omega}_e \tag{21}$$

The selected full-order sliding mode surface is

$$s_1 = \dot{x}_1 + c_1 \mathrm{sgn}(x_1)|x_1|^{\mu_1} \tag{22}$$

where $c_1 > 0$, and the selection of μ_1 is determined by (11).

Substituting (21) into (22) and combining it with (9) and (12) yields

$$u_{c1} = -\dot{x}_1 = -(u_{eq1} + u_{st1}) \tag{23}$$

The equivalent control law u_{eq1} of FOMFSMC is given as follows:

$$u_{eq1} = -c_1 \mathrm{sign}(x_1)|x_1|^{\mu_1} \tag{24}$$

The switching control law u_{st1} is given as follows:

$$\dot{u}_{st1} + T_1 u_{st1} = v_1 \tag{25}$$

$$v_1 = -k_1 \mathrm{sgn}(s_1) - k_2 s_1 \tag{26}$$

where $k_1 > 0$, $k_2 > 0$, and $T_1 > 0$.

Proof 1 *For the stability analysis of the FOMFSMC, substituting (23) and (24) into (22) yields*

$$s_1 = u_{st1} \tag{27}$$

The Lyapunov function V_1 is selected as

$$V_1 = \frac{1}{2} s_1^2 \tag{28}$$

Differentiating (28) yields

$$\begin{aligned} \dot{V}_1 &= s_1 \dot{s}_1 = s_1 \dot{u}_{st1} = s_1 (v_1 - T_1 u_{st1}) \\ &= s_1 (-k_1 \mathrm{sgn}(s_1) - k_2 s_1 - T_1 s_1) \\ &= -k_1 |s_1| - k_2 s_1^2 - T_1 s_1^2 \end{aligned} \tag{29}$$

It is evident that the inequality $\dot{V}_1 \leq 0$ is satisfied when $k_1 > 0$, $k_2 > 0$, and $T_1 > 0$. The system's asymptotic stability is guaranteed using Lyapunov stability theory and the sliding-mode reachability condition, and the state error converges to zero in finite time.

Substituting (23) through (26) into (17) yields

$$i_{q1}^* = \frac{1}{\gamma} \left[\begin{array}{l} \dot{\omega}_e^* - \xi \omega_\mathrm{e} - F_1 + c_1 \mathrm{sgn}(x_1)|x_1|^{\mu_1} \\ + \frac{1}{T_1} (k_1 \mathrm{sgn}(s_1) + k_2 s_1 + \dot{u}_{st1}) \end{array} \right] \tag{30}$$

3.3. Design of ESMDO

With the actual input and output data from the system, the ESMDO performs real-time estimation of the unknown disturbance, while providing feedforward compensation to the sliding mode controller, thereby strengthening system robustness.

Substituting the sliding mode observer control law into (6) yields [9]:

$$\begin{cases} \dfrac{\mathrm{d}\hat{\omega}_\mathrm{e}}{\mathrm{dt}} = \hat{F}_1 + \gamma i_q + \xi \hat{\omega}_e + u_{\mathrm{smo1}} \\ \dfrac{\mathrm{d}\hat{F}_1}{\mathrm{dt}} = G_1 \cdot u_{\mathrm{smo1}} \end{cases} \tag{31}$$

where u_{smo1} denotes the sliding mode control law; G_1 is the corresponding coefficient; and $\hat{\omega}_e$ and $\hat{F}_1$ represent the observed values of ω_e and F_1, respectively.

Combining (17) and (31) yields the dynamic error equation of the ESMDO as follows:

$$\begin{cases} \dot{z}_1 = \xi z_1 + \tilde{F}_1 + u_{\mathrm{smo}} \\ \dot{\tilde{F}} = G \cdot u_{\mathrm{smo1}} - \delta(t) \end{cases} \tag{32}$$

where the error in the speed observation is denoted by $z_1 = \hat{\omega}_e - \omega_e$; the observation error of the unknown total disturbance is represented by $\tilde{F}_1 = \hat{F}_1 - F_1$; and $\delta(t) = dF/dt$.

The speed observation error z_1 is selected as the state variable, and the sliding mode surface is defined as:

$$s_2 = z_1 = \hat{\omega}_e - \omega_e \tag{33}$$

The exponential reaching law is selected as

$$\dot{s}_2 = -n_1 \mathrm{sgn}(s_2) - n_2 s_2 \tag{34}$$

where n_1 and n_2 are positive constants.

Substituting (32) into (34), the sliding mode function to be designed is expressed as

$$u_{\mathrm{smo1}} = -\xi z_1 - n_1 \mathrm{sgn}(s_2) - n_2 s_2 \tag{35}$$

Proof 2 *For the stability analysis of the ESMDO, Lyapunov function V_2 is selected as*

$$V_2 = \frac{1}{2} {s_2}^2 \tag{36}$$

Differentiating (36) yields

$$\begin{aligned} \dot{V}_2 &= s_2 \dot{s}_2 = z_1(\xi z_1 + \tilde{F}_1 + u_{\mathrm{smo1}}) \\ &= z_1(\tilde{F}_1 - n_1 \mathrm{sgn}(s_2) - n_2 s_2) \\ &= z_1 \tilde{F}_1 - n_1 z_1 \mathrm{sgn}(z_1) - n_2 z_1^2 \\ &\leq z_1 \tilde{F}_1 - n_1 z_1 \mathrm{sgn}(z_1) \\ &\leq \parallel z_1 \parallel \left(\parallel \tilde{F}_1 \parallel - n_1 \right) \end{aligned} \tag{37}$$

When gains are selected such that $n_1 \geq \parallel \tilde{F}_1 \parallel$ and $\dot{V}_2 \leq 0$, the system is asymptotically stable, and its observation error z_1 converges to zero within a finite time.

By substituting (35) into (31), the expression for the estimate of the total disturbance $\hat{F}_1$ is given as

$$\hat{F}_1 = G_1 \int (-\xi z_1 - n_1 \mathrm{sgn}(s_2) - n_2 s_2)\, dt \tag{38}$$

Substituting the observed value $\hat{F}_1$ into (30) yields the total control law of the FOMFSMC system, which can be expressed as

$$i_{q1}^* = \frac{1}{\gamma} \left[\begin{array}{l} \dot{\omega}_e^* - \xi \omega_e - \hat{F}_1 + c_1 \mathrm{sgn}(x_1)|x_1|^{\mu_1} \\ + \frac{1}{T_1} (k_1 \mathrm{sgn}(s_1) + k_2 s_1 + \dot{u}_{st1}) \end{array} \right] \tag{39}$$

4. DESIGN OF IFOMFSMC BASED ON FOESMDO

To reduce the speed overshoot and steady-state error of the system, the IFOMFSMC was designed by further improving the full-order sliding mode controller. Moreover, the FOSMC is introduced into the extended disturbance observer to further enhance the speed-tracking performance and disturbance-rejection capability.

4.1. Design of IFOMFSMC

The state error is defined by (19) as follows:

$$x_2 = e = \omega_e^* - \omega_e \tag{40}$$

The speed error is selected as the controller state variable as follows:

$$\begin{cases} x_2 = \omega_e^* - \omega_e \\ \dot{x}_2 = -u_{c2} = \dot{\omega}_e^* - \dot{\omega}_e \\ \ddot{x}_2 = -\dot{u}_{c2} = \ddot{\omega}_e^* - \ddot{\omega}_e \end{cases} \tag{41}$$

By establishing a relationship between the control voltage and sliding mode surface, the system's dynamic and steady-state performance can be enhanced simultaneously [17]. Introducing the term $\ddot{x}_2$ into the sliding mode surface improves the steady-state accuracy of the speed control system. Based on this, a second-order full-order sliding surface s_3 is formulated as follows:

$$s_3 = \ddot{x}_2 + c_3 \mathrm{sgn}(\dot{x}_2)|\dot{x}_2|^{\mu_3} + c_2 \mathrm{sgn}(x_2)|x_2|^{\mu_2} \tag{42}$$

where $c_2 > 0$ and $c_3 > 0$. μ_2 and μ_3 are selected using (11).

An improved double-power reaching law [18] is introduced to accelerate the system's response speed and enhance chattering suppression. Substituting (41) into (42) and combining it with (9) and (12) yields

$$\dot{u}_{c2} = -\ddot{x}_2 = -(u_{eq2} + u_{st2}) \tag{43}$$

$$u_{c2} = \int -(u_{eq2} + u_{st2})dt \tag{44}$$

From (44), it can be observed that by introducing $\ddot{x}_2$ into the sliding mode surface, the controller as a whole becomes an integral term, thereby reducing the steady-state error associated with the controller.

The equivalent control law u_{eq2} is given as follows:

$$u_{eq2} = -c_3 \mathrm{sgn}(\dot{x}_2)|\dot{x}_2|^{\mu_3} - c_2 \mathrm{sgn}(x_2)|x_2|^{\mu_2} \tag{45}$$

The switching control law u_{st2} is given as follows:

$$\dot{u}_{st2} + T_2 u_{st2} = v_2 \tag{46}$$

$$v_2 = -k_3(|x_2|\,|s_3|)^{1-\lambda}\mathrm{sgn}(s_3) - k_4|s_3|^{1+\lambda}\mathrm{sgn}(s_3) \tag{47}$$

Proof 3 *For the stability analysis of the IFOMFSMC, substituting (44) and (45) into (42) yields*

$$s_3 = u_{st2} \tag{48}$$

The Lyapunov function V_3 is selected as

$$V_3 = \frac{1}{2}s_3^2 \tag{49}$$

Differentiating (49) yields

$$\begin{aligned} \dot{V}_3 &= s_3\dot{s}_3 = s_3\dot{u}_{st2} \\ &= s_3(v_2 - T_2u_{st2}) = s_3\Big(-k_3(|x_2|\,|s_3|)^{1-\lambda}\mathrm{sgn}(s_3) \\ &\quad -k_4|s_3|^{1+\lambda}\mathrm{sgn}(s_3) - T_2 s_3\Big) \\ &= -k_3(|x_2|\,|s_3|)^{1-\lambda}|s_3| - k_4|s_3|^{2+\lambda} - T_2 s_3^2 \\ &= -k_3|x_2|^{1-\lambda}|s_3|^{2-\lambda} - k_4|s_3|^{2+\lambda} - T_2 s_3^2 \end{aligned} \tag{50}$$

It is evident that the inequality $\dot{V}_3 \leq 0$ is satisfied when $k_3 > 0$, $k_4 > 0$, $T_2 > 0$, and $0 < \lambda < 1$. The asymptotic stability of the system is guaranteed by Lyapunov stability theory and the sliding-mode reachability condition, and the state error converges to zero within finite time.

Substituting (43)–(47) into (17) yields the control law for i_{q2}^* in the IFOMFSMC as follows:

$$i_{q2}^* = \frac{1}{\gamma}\left[\begin{array}{l} \dot{\omega}_e^* - \xi\omega_e - F_2 \\ + \displaystyle\int \left(\begin{array}{l} c_3\mathrm{sgn}(\dot{x}_2)|\dot{x}_2|^{\mu_3} + c_2\mathrm{sgn}(x_2)|x_2|^{\mu_2} \\ + \dfrac{1}{T_2}\left(\begin{array}{l} k_3(|x_2|\,|s_3|)^{1-\lambda}\mathrm{sgn}(s_3) + \\ k_4|s_3|^{1+\lambda}\mathrm{sgn}(s_3) + \dot{u}_{st2} \end{array}\right) \end{array}\right) dt \end{array}\right] \tag{51}$$

Figure 1 shows a block diagram of the designed IFOMFSMC.

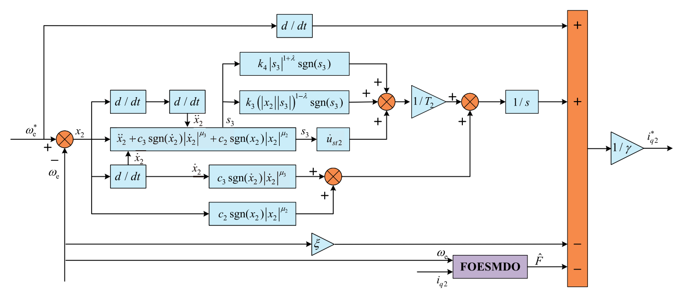

FIGURE 1. The block diagram of the IFOMFSMC algorithm.

4.2. Design of FOESMDO

An FOSMC is introduced into an ESMDO to strengthen IFOMFSMC's disturbance-rejection capability and speed-tracking performance.

Similar to the design of the ESMDO, an observer is constructed as follows:

$$\begin{cases} \dfrac{\mathrm{d}\hat{\omega}_e}{\mathrm{d}t} = \hat{F}_2 + \gamma i_{q2} + \xi\hat{\omega}_e + u_{\mathrm{smo2}} \\ \dfrac{\mathrm{d}\hat{F}_2}{\mathrm{d}t} = G_2 \cdot u_{\mathrm{smo2}} \end{cases} \tag{52}$$

where the observed value of ω_e is denoted by $\hat{\omega}_e$; the observed value of F_2 is denoted by $\hat{F}_2$; G_2 represents the coefficient of the sliding mode control law, and the sliding mode control law is written as u_{smo2}.

With the observation error chosen as the state variable, the dynamic error state equation of the observer can be written as follows:

$$\begin{cases} z_2 = \hat{\omega}_e - \omega_e \\ \dot{z}_2 = \xi z_2 + \tilde{F}_2 + u_{\mathrm{smo2}} \\ \dot{\tilde{F}}_2 = G_2 \cdot u_{\mathrm{smo2}} - \ell(t) \end{cases} \tag{53}$$

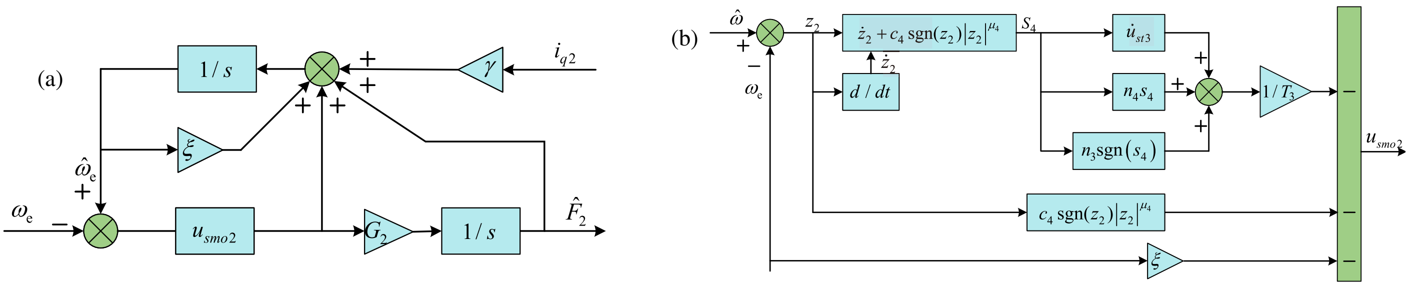

FIGURE 2. Block diagram of the FOESMDO algorithm. (a) Block diagram of the overall FOESMDO structure and (b) block diagram of the u_{smo2} control law.

where $\ell(t)$ denotes the time derivative of the unknown total disturbance, and $\tilde{F}_2 = \hat{F}_2 - F_2$ represents the error in its observation.

The full-order sliding mode surface s_4 is chosen, which can be written as

$$s_4 = \dot{z}_2 + c_4\mathrm{sgn}(z_2)|z_2|^{\mu_4} \tag{54}$$

where $c_4 > 0$, and the selection of μ_4 is determined by (9).

Substituting (53) into (54) and combining (9) and (12) yields

$$u_{\mathrm{smo2}} = u_{eq3} + u_{st3} \tag{55}$$

The equivalent control law u_{eq3} is given as follows:

$$u_{eq3} = -\xi z_2 - c_4\mathrm{sgn}(z_2)|z_2|^{\mu_4} \tag{56}$$

The switching control law u_{st3} is given as follows:

$$\dot{u}_{st3} + T_3 u_{st3} = v_3 \tag{57}$$

$$v_3 = -n_3\mathrm{sgn}(s_4) - n_4 s_4 \tag{58}$$

where $T_3 > 0$, $n_3 > 0$, and $n_4 > 0$.

Substituting (55)–(58) into (52) yields the expression for the total disturbance estimate $\hat{F}_2$ as follows:

$$\hat{F}_2 = G_2 \int \begin{bmatrix} -\xi z_2 - c_4\mathrm{sgn}(z_2)|z_2|^{\mu_4} \\ -\frac{1}{T_3}\left(n_3\mathrm{sgn}(s_4) + n_4 s_4 + \dot{u}_{st3}\right) \end{bmatrix} dt \tag{59}$$

Figure 2 shows a detailed block diagram of the designed FOESMDO.

Theorem 1 *When there exist parameters n_{d1} and n_{d2} such that $n_3 = n_{d1} + n_{d2}$, and $n_{d1} \geq |\dot{\tilde{F}}_2|$, $n_{d2} \geq T_3|\tilde{F}_2|$, the state error in (53) converges to zero in a finite time.*

Proof 4 *Substituting (55) and (56) into (54) yields*

$$s_4 = \tilde{F}_2 + u_{st3} \tag{60}$$

The Lyapunov function V_4 is selected as

$$V_4 = \frac{1}{2}s_4^2 \tag{61}$$

Differentiating (61)

$$\begin{aligned} \dot{V}_4 &= s_4\dot{s}_4 = s_4\left(\dot{\tilde{F}}_2 + \dot{u}_{st3}\right) = s_4\left(\dot{\tilde{F}}_2 + v_3 - T_3 u_{st3}\right) \\ &= s_4\left(\dot{\tilde{F}}_2 - n_3\mathrm{sgn}(s_4) - n_4 s_4 - T_3 u_{st3}\right) \\ &= s_4\dot{\tilde{F}}_2 - n_3|s_4| - n_4 s_4^2 - T_3\left(s_4 - \tilde{F}_2\right)s_4 \\ &\leq \left(s_4\dot{\tilde{F}}_2 - n_{d1}|s_4|\right) + \left(s_4 T_3\tilde{F}_2 - n_{d2}|s_4|\right) \\ &\quad -n_4 s_4^2 - T_3 s_4^2 \end{aligned} \tag{62}$$

It is apparent that under conditions $n_{d1} \geq |\dot{\tilde{F}}_2|$ and $n_{d2} \geq T_3|\tilde{F}_2|$, the inequality $\dot{V}_4 \leq 0$ holds. According to the Lyapunov stability theorem and sliding-mode reaching condition, we conclude that the system achieves asymptotic stability and that the observation error z_2 tends to zero within a finite time.

By substituting the observed value $\hat{F}_2$ into (51), the following expression for the overall control law of the IFOMFSMC system is obtained:

$$i_{q2}^* = \frac{1}{\gamma}\begin{bmatrix} \dot{\omega}_e^* - \xi\omega_e - \hat{F}_2 \\ + \displaystyle\int \begin{pmatrix} c_3\mathrm{sgn}(\dot{x}_2)|\dot{x}_2|^{\mu_3} + c_2\mathrm{sgn}(x_2)|x_2|^{\mu_2} \\ + \dfrac{1}{T_2}\begin{pmatrix} k_3(|x_2|\,|s_3|)^{1-\lambda}\mathrm{sgn}(s_3) + \\ k_4|s_3|^{1+\lambda}\mathrm{sgn}(s_3) + \dot{u}_{st2} \end{pmatrix} \end{pmatrix} dt \end{bmatrix} \tag{63}$$

5. SIMULATION VERIFICATION

To verify the effectiveness of the proposed method, the FOMFSMC and IFOMFSMC models were first implemented in MATLAB/Simulink and compared with the conventional MFSMC; the results confirmed that the actual speed under the proposed algorithm could track the reference speed. Subsequent comparisons with the PI under different disturbance conditions showed significantly improved performance indicators. Figure 3 presents a block diagram that summarizes the PMSM speed control system.

For the PMSM, the currents on the d-q axis were regulated using the MTPA control strategy. The intersection of the MTPA curve and the current limit circle defines their respective limiting ranges: $[-43.83, 0]$ for the d axis and $[0, 54.58]$ for the q axis.

The speed responses of the FOMFSMC and conventional MFSMC were compared using the method of controlling variables. In the conventional control, the observer is the same ESMDO as in the FOMFSMC, whereas the controller adopts a non-singular fast terminal sliding surface $\mathbf{s} = \mathbf{e}_1 + \alpha\mathbf{e}_1^{g/h} + \beta\mathbf{e}_2^{p/q}$ and an exponential reaching law

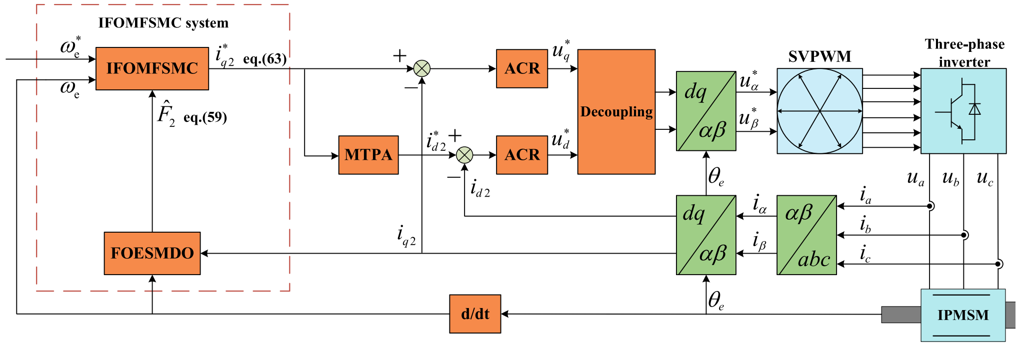

FIGURE 3. The block diagram of the PMSM speed control system.

TABLE 1. The parameters of PMSM.

Parameters	Unit	Value
DC voltage (u_{dc})	V	600
Rated current (i_s)	A	70
Rated speed (n_N)	r/min	1900
q axis stator inductance (L_q)	H	0.009
d axis stator inductance (L_d)	H	0.004
Stator resistance (R_s)	Ω	2.75
Rotor PM flux (ψ_f)	Wb	0.12
Viscous friction coefficient (B_m)	$\mathrm{N \cdot m \cdot s/rad}$	0.001
Rotational inertia (J)	$\mathrm{kg \cdot m^2}$	0.029
Number of pole pairs (n_p)	pairs	2

TABLE 2. Parameters of the four control algorithms.

PI	NFTSMC	FOMFSMC	IFOMFSMC
$P = 50$	$g/h = 5/3$	$\mu_1 = 0.75$	$\mu_2 = 0.6$
$I = 50$	$p/q = 7/5$	$c_1 = 400$	$\mu_3 = 0.75$
	$\alpha = 0.1$	$k_1 = 17000$	$c_2 = 120000$
	$\beta = 0.001$	$k_2 = 0.75$	$c_3 = 2310$
	$k_5 = 25$	$T_1 = 5$	$\lambda = 0.45$
	$k_6 = 25$	$n_1 = 13330$	$k_3 = 20$
	$n_5 = 2000$	$n_2 = 1250$	$k_4 = 2 \cdot 10^{-6}$
	$n_6 = 25000$	$G_1 = 4$	$T_2 = 20$
	$G_3 = 4$		$\mu_4 = 0.8$
			$c_4 = 30000$
			$n_3 = 50000$
			$n_4 = 8000$
			$T_3 = 20$
			$G_2 = 4$

$\dot{s} = -k_5 \mathrm{sign}(s) - k_6 s$, where $\dot{e}_1 = e = e_2$ on the sliding mode surface.

The PMSM parameters are listed in Table 1.

The parameters of the four control methods used in the simulation are presented in Table 2. In the control algorithm, the values of γ and ξ are determined by $\gamma = 3n_p^2\psi_{\text{ext}}/2J$ and $\xi = -B/J$. Before adjusting the parameters of the IFOMFSMC algorithm, the controller's outermost integrator was precisely limited to a saturation range of $[-54.58\gamma, 54.58\gamma]$. Consequently, after the appropriate parameters are obtained, the speed overshoot was significantly reduced. Parameters c_2 and c_3 directly govern the convergence rate and dynamic quality during the sliding-mode motion. A larger c_2 accelerates convergence but may cause a large transient overshoot, whereas reducing c_2 slows the response and prolongs the settling time. The effect of c_3 was opposite. In practice, both are initially chosen as large as possible subject to $c_2 < 5c_3$ and then tuned according to the steady-state error and robustness requirements. The selection of k_3, k_4, and T_2 also affects the time required for the sliding mode surface to stabilize. Increasing T_2 slows the system response, whereas decreasing T_2 allows the motor to reach the reference speed faster but increases the steady-state error. After T_2 is determined, k_3 and k_4 are tuned. Increasing k_3 and k_4 accelerates the dynamic response and shortens the time to reach the sliding surface, but may cause larger overshoot and increased steady-state speed error in the PMSM system. In the observer, c_4, n_3, n_4, and T_3 govern the steady-state error and robustness, and are tuned using the same principle as that of the controller. The gain G_2 directly determines the observed disturbance F_2 that is fed back to the controller as compensation: a larger G_2 enhances robustness to parameter variations and external disturbances at the cost of an increased speed tracking error, whereas a smaller G_2 reduces the tracking error but weakens the robustness.

5.1. Simulation Verification of Speed Accuracy

In the simulation, the PMSM operated at a constant load of $T_L = 15\,\mathrm{N \cdot m}$. The reference speed of the PMSM was set as follows: at $t = 0\,\mathrm{s}$, $n_f = 300\,\mathrm{r/min}$; at $t = 0.4\,\mathrm{s}$, $n_f = 900\,\mathrm{r/min}$; and at $t = 0.8\,\mathrm{s}$, $n_f = 1800\,\mathrm{r/min}$. Figure 4 presents the speed response waveforms of the conventional model-free sliding mode control and the two full-order model-free sliding mode control methods.

As shown in enlarged views 1, 2, and 3 in Figure 4, in three different reference speeds, the actual speeds of both IFOMFSMC and FOMFSMC can reach corresponding reference speeds, whereas those of NFTSMC can not. Furthermore, the deviation between the reference and actual speeds of the PMSM varied as the reference speed changed. The simulation results demonstrate that the control system with FOMFSMC and IFOMFSMC exhibits good speed-regulation capability.

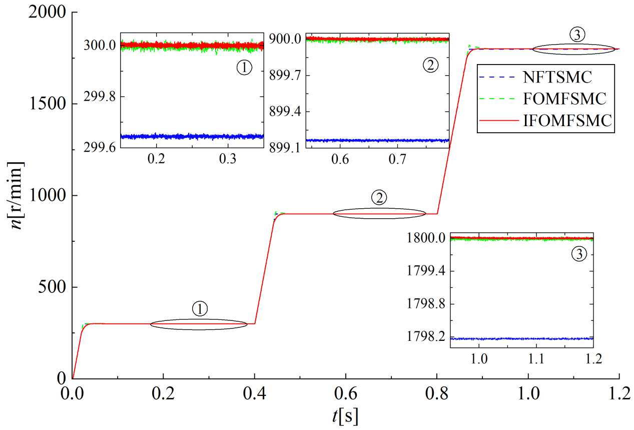

FIGURE 4. Comparison of speed accuracy.

5.2. Simulation Results under Single Time-Varying Disturbance Conditions

Under the single time-varying disturbance condition, only one parameter is perturbed at any given time. The load torque was initially set to $T_L = 15\,\text{N} \cdot \text{m}$, and the reference speed is set to $n_f = 900\,\text{r/min}$. At 0.65 s, the speed was changed to $n_f = 1800\,\text{r/min}$. To evaluate the tracking and disturbance rejection capabilities of the three control strategies PI, FOMFSMC, and IFOMFSMC, the key PMSM parameters, including n_f, ψ_f, B_m, L_q, L_d, and T_L are perturbed. The parameter perturbation conditions are presented in Table 3.

TABLE 3. Perturbation range of parameters.

Time/s	Parameters	Range of Perturbations
1.3 s	$n_f/\text{r} \cdot \text{min}^{-1}$	1800→1800+50sin5πt
2.3 s	$n_f/\text{r} \cdot \text{min}^{-1}$	1800+50sin5πt→1800
2.8 s	ψ_f/Wb	0.12→0.09
3.3 s	$B_m/(\text{N} \cdot \text{m} \cdot \text{s/rad})$	0.001→0.004
3.8 s	L_q/H	0.009→0.006
4.3 s	L_d/H	0.004→0.003
4.8 s	$T_L/\text{N} \cdot \text{m}$	15→20
5.3 s	$T_L/\text{N} \cdot \text{m}$	20→20+4sin4πt
6.3 s	$T_L/\text{N} \cdot \text{m}$	20+4sin4πt→20

Figure 5 presents the simulation results for the PI, FOMFSMC, and IFOMFSMC methods. These figures clearly show a comparison of the response speed, speed overshoot, steady-state error, tracking capability, disturbance rejection, and torque ripple.

As shown in Figures 5(a) and 5(b), under a single time-varying disturbance, the proposed IFOMFSMC exhibits the fastest dynamic response during the two speed intervals, 0 to 900 r/min and 900 to 1800 r/min. It reached the reference speed with an overshoot of only 0.11 r/min and entered the steady state at 0.088 and 0.74 s, respectively. In contrast, the FOMFSMC settled at 0.128 and 0.778 s, whereas the PI required 0.32 and 0.975 s. Both FOMFSMC and PI showed significant overshoot. Compared with PI, the response speed of the IFOMFSMC is improved by 72.5% and 72.3% in the two stages. At 1.3 s, a periodic time-varying speed command was applied. Both the IFOMFSMC and FOMFSMC can closely track the command, with steady-state errors of 0.025 r/min and 0.06 r/min, respectively. However, the PI failed to follow effectively, with a tracking error of 0.17 r/min. IFOMFSMC tracking accuracy was improved by 85.3% over the PI.

The three methods exhibited markedly different disturbance rejection capabilities. At 2.8 s, a disturbance of ψ_f was applied. The FOMFSMC and PI exhibited maximum speed drops of 0.185 r/min and 0.241 r/min, recovering in 0.01 s and 0.14 s, respectively. In contrast, the IFOMFSMC dropped only 0.126 r/min and recovered within 0.004 s. At 3.3 s, a disturbance in B_m occurred. The PI speed dropped by 0.072 r/min and recovered in 0.051 s, whereas the IFOMFSMC and FOMFSMC speeds remained stable. At 3.8 s, a disturbance in L_q was introduced. The FOMFSMC and PI dropped by 0.529 r/min and 0.765 r/min, recovering in 0.011 s and 0.205 s, respectively. The IFOMFSMC dropped only 0.403 r/min and recovered within 0.005 s. At 4.3 s, a disturbance of L_d was applied. The FOMFSMC and PI dropped by 0.165 r/min and 0.352 r/min, recovering in 0.005 s and 0.175 s, respectively. The IFOMFSMC dropped only 0.163 r/min and recovered within 0.003 s. At 4.8 s, a disturbance in T_L occurs. The FOMFSMC and PI exhibited maximum speed drops of 0.391 r/min and 0.595 r/min with recovery times of 0.012 s and 0.198 s, respectively. The IFOMFSMC dropped only 0.36 r/min and recovered within 0.004 s. At 5.3 s, a periodic time-varying T_L command was applied. The PI speed exhibited large fluctuations, whereas the IFOMFSMC and FOMFSMC maintained the reference speed without significant variation.

As shown in Figure 5(c), the proposed IFOMFSMC effectively suppresses torque ripple. Its torque ripple during both steady-state operation and dynamic tracking was smaller than that of the FOMFSMC and PI.

As shown in Figure 5(d), all three control methods, namely IFOMFSMC, FOMFSMC, and PI, are capable of operating along the MTPA curve. However, comparing the adherence and smoothness of the trajectories, it was observed that the IFOMFSMC achieved the highest tracking accuracy with respect to the MTPA curve, and its current trajectory exhibited the smallest deviation from the theoretical curve. Specifically, during both steady-state and dynamic processes, the magnitudes of the d-axis and q-axis current ripples generated by the IFOMFSMC were significantly lower than those produced by the FOMFSMC and PI. Consequently, the IFOMFSMC has superior harmonic suppression and disturbance rejection, thereby a smoother current trajectory and better control performance than the FOMFSMC.

As shown in Figures 5(e) and 5(f), the simulation results of the ESMDO and FOESMDO are compared. The results demonstrate that, with the same reaching law, the FOESMDO, which incorporates a full-order sliding-mode structure, exhibits superior comprehensive performance. The FOESMDO's tracking accuracy for unknown system disturbances is significantly improved, and the tracking error is markedly reduced. Furthermore, the estimation error of the disturbance output by the FOESMDO is smaller, and the chattering in the observer sig-

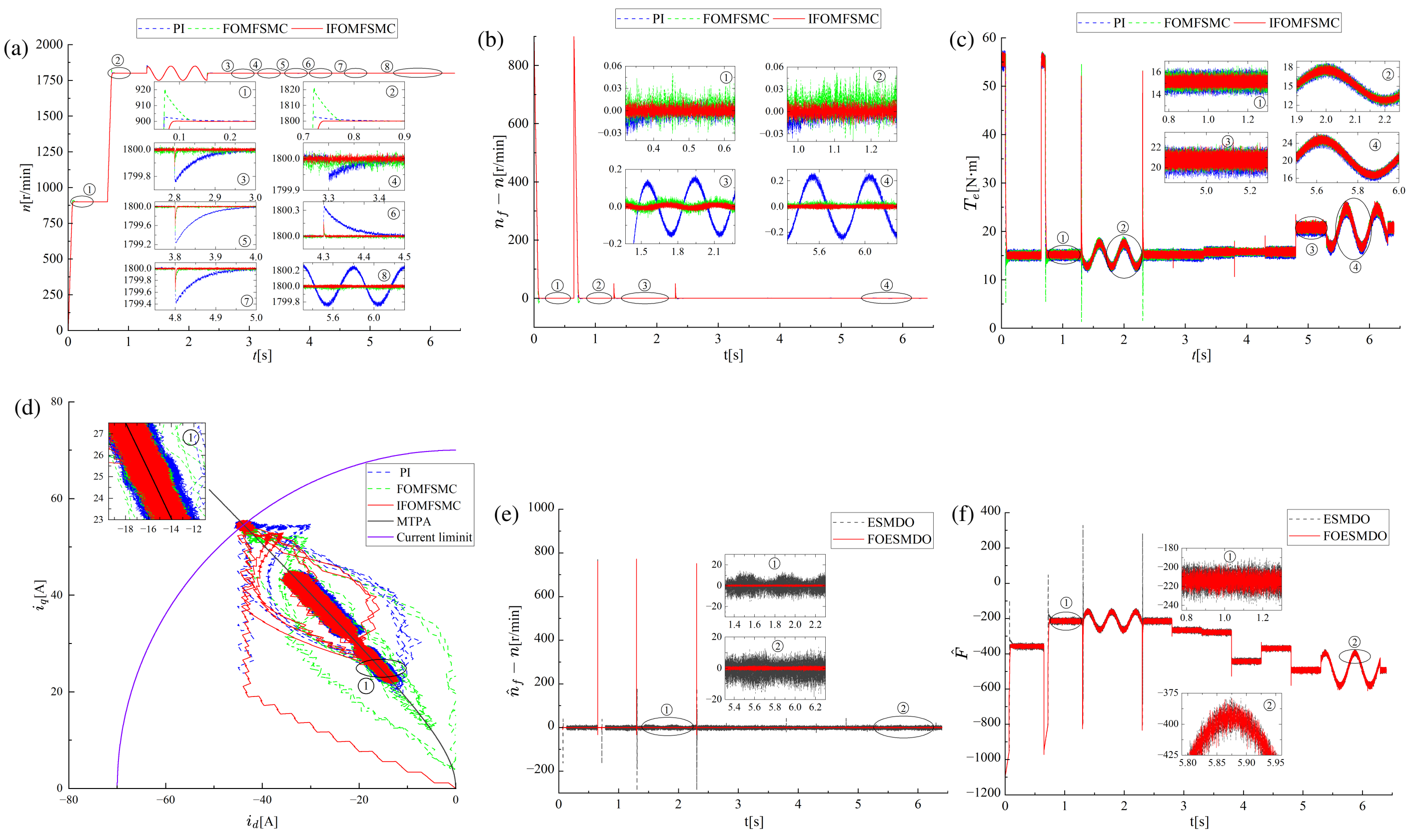

FIGURE 5. The simulation results under single time-varying disturbance operating conditions. (a) Simulation results of speed, (b) simulation results of speed error $n_f - n$, (c) simulation results of torque, (d) the current trajectory of i_d and i_q, (e) observed speed tracking error $\hat{n}_f - n$, and (f) observed value of the unknown disturbance.

nal is effectively attenuated. Consequently, the FOESMDO's output becomes smoother, providing more accurate disturbance compensation for the controller.

In summary, under a single time-varying disturbance condition, the proposed IFOMFSMC consistently outperformed both the FOMFSMC and the PI across all evaluated performance indicators, clearly demonstrating superior dynamic response, reduced steady-state error, enhanced disturbance rejection, and lower torque ripple.

5.3. Simulation Results under Complex Time-Varying Disturbance Conditions

Under complex time-varying disturbance conditions, multiple parameters undergo time-varying perturbations simultaneously. Considering the inherent uncertain disturbances caused by factors such as environmental variations under complex practical operating conditions, the load torque and PMSM parameters are no longer constant. Therefore, under such conditions, complex time-varying disturbances are generated by adding a sinusoidal time-varying disturbance together with two white noise sequences, which are produced by the random module in Simulink, to each parameter of the PMSM. The parameters of the complex time-varying disturbances are listed in Table 4, where the entries in the Noise column represent the variances output by the random module.

The load torque was initially set to $T_L = 15\,\mathrm{N \cdot m}$, and the reference speed was set to $n_f = 1800\,\mathrm{r/min}$. Complex time-varying disturbances are introduced to the load torque, PMSM parameters, and reference speed. Table 5 lists the PMSM ranges of multi-parameter disturbances in the simulation model.

TABLE 4. Parameters of complex time-varying disturbances.

Parameters	Perturbations	Noise 1	Noise 2
T_D	$3.2 \cdot 10^{-1}$sin225πt	$1 \cdot 10^{-4}$	$2 \cdot 10^{-2}$
ψ_D	$9.6 \cdot 10^{-3}$sin(225πt+30)	$1 \cdot 10^{-7}$	$7.5 \cdot 10^{-6}$
R_D	$9 \cdot 10^{-2}$sin(225πt+60)	$5 \cdot 10^{-6}$	$8 \cdot 10^{-5}$
L_{qD}	$3.6 \cdot 10^{-4}$sin(225πt+90)	$6 \cdot 10^{-10}$	$3 \cdot 10^{-8}$
L_{dD}	$2.4 \cdot 10^{-4}$sin(225πt+120)	$4 \cdot 10^{-10}$	$5 \cdot 10^{-9}$
J_D	$1.2 \cdot 10^{-3}$sin(225πt+150)	$4 \cdot 10^{-9}$	$4 \cdot 10^{-7}$
B_D	$6 \cdot 10^{-5}$sin(225πt+180)	$4 \cdot 10^{-12}$	$2 \cdot 10^{-10}$

The comparison results of the PI, FOMFSMC, and IFOMFSMC under complex time-varying disturbance conditions are presented in Figure 6 to comprehensively evaluate the performance of different control methods.

As shown in Figures 6(a) and 6(b), under complex time-varying disturbance conditions, T_L begins to exhibit complex time-varying disturbances from 0 s. With a reference speed of 1800 r/min, the proposed IFOMFSMC reached the reference speed with a speed overshoot of 0.09 r/min and entered the steady state at 0.159 s. In contrast, the FOMFSMC and PI settled at 0.261 s and 0.375 s, respectively, both with obvious over-

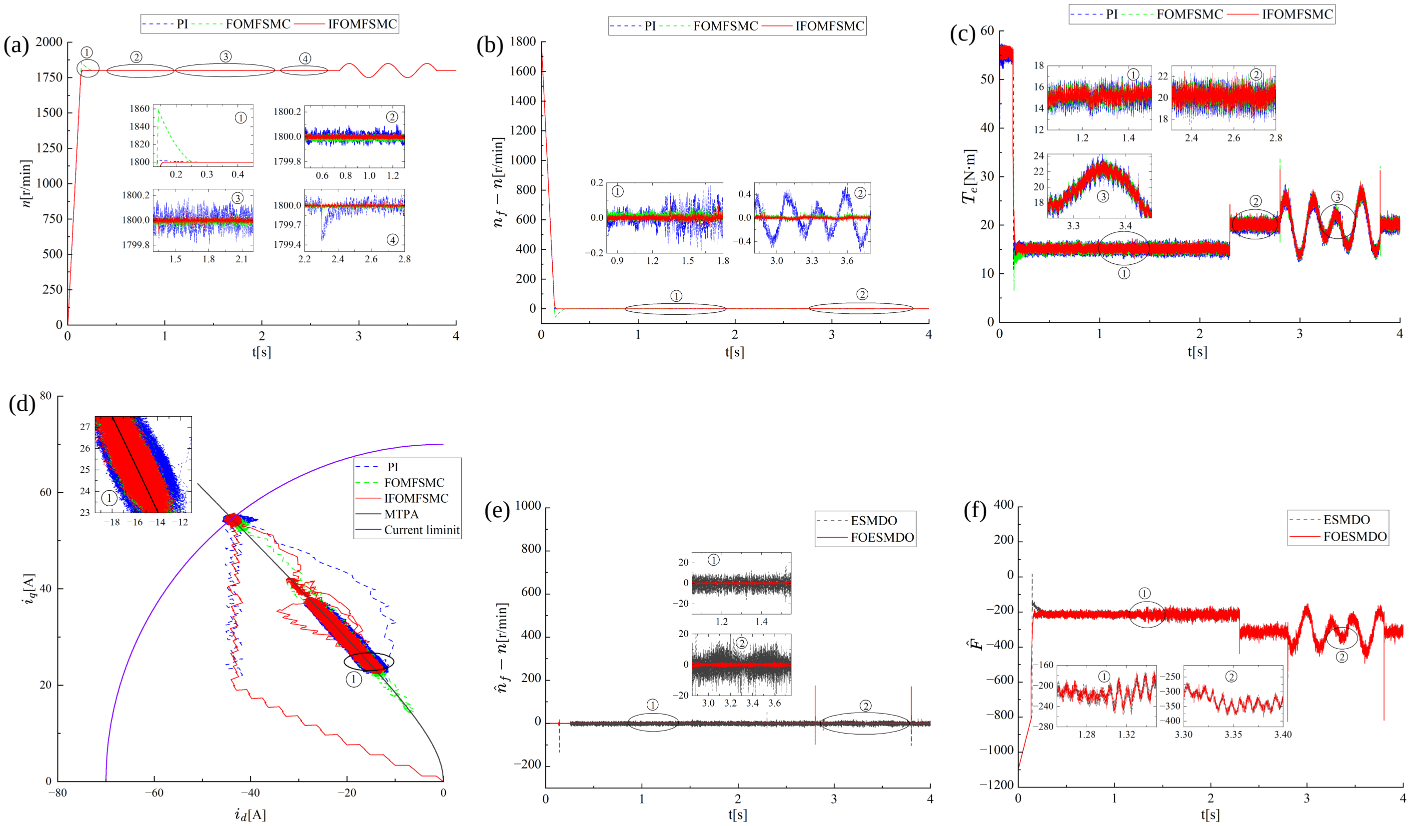

FIGURE 6. Simulation results under the condition of complex time-varying disturbance. (a) Simulation results of speed, (b) simulation results of speed error $n_f - n$, (c) simulation results of torque, (d) the current trajectory of i_d and i_q, (e) observed speed tracking error $\hat{n}_f - n$, and (f) observed value of the unknown disturbance.

TABLE 5. Range of complex time-varying parameter perturbations.

Time/s	Parameters	Range of Perturbations
0 s	T_L/(N·m)	0→15+T_D
1.3 s	ψ_f/Wb	0.12→0.12+ψ_D
	R_s/Ω	2.75→2.75+R_D
	L_q/H	0.009→0.009+L_{qD}
	L_d/H	0.004→0.004+L_{dD}
	J/(kg·m^2)	0.029→0.029+J_D
	B_m/(N·m·s/rad)	0.001→0.001+B_D
2.3 s	T_L/(N·m)	15+T_D·20+T_D
2.8 s	T_L/(N·m)	20+T_D→20+4sin8πt+T_D
	$n_f/\mathrm{r\cdot min^{-1}}$	1800→1800+50sin(5πt-30)
3.8 s	T_L/(N·m)	20+4sin8πt+T_D→20+T_D
	$n_f/\mathrm{r\cdot min^{-1}}$	1800+50sin(5πt-30)→1800

shoot. In the steady state, the steady-state error of the IFOMFSMC was only 0.025 r/min, compared with 0.05 r/min for the FOMFSMC and 0.081 r/min for the PI. In this speed interval, the IFOMFSMC response speed improved by 57.6% over PI, and steady-state error was reduced by 69.1%.

At 1.3 s, all parameters of PMSM undergo complex time-varying parameter perturbations. The PI steady-state error then increased to 0.181 r/min, whereas the IFOMFSMC and FOMFSMC errors were only 0.051 and 0.064 r/min. The IFOMFSMC steady-state error is reduced by 71.8% compared with that of PI. When T_L changed at 2.3 s, the FOMFSMC and PI speeds dropped by 0.451 and 0.541 r/min, and recovered in 0.011 s and 0.149 s. In contrast, the IFOMFSMC dropped only 0.391 r/min and recovered in 0.004 s. At 2.8 s, when a wide-range time-varying command is applied to both n_f and T_L of the PMSM, the PI fails to track the reference. Compared with the case in which only the reference speed varied, the tracking error of the PI increased significantly to 0.535 r/min. However, the IFOMFSMC and FOMFSMC tracked in real time, with errors of only 0.063 and 0.095 r/min. The IFOMFSMC tracking capability was improved by 88.2% over PI.

As shown in Figure 6(c), the output torque ripple of the IFOMFSMC is less than that of the FOMFSMC and PI under both steady-state and dynamic conditions. Specifically, when the load torque was 20 N · m, the torque ripple of the IFOMFSMC is only 1.38 N · m, whereas those of the FOMFSMC and the PI are 1.79 N·m and 1.95 N·m, respectively. The torque ripple of the IFOMFSMC was reduced by 29.2% compared with that of the PI.

As shown in Figure 6(d), under complex disturbance conditions, the current trajectories of the d-q axes of the three control methods are driven along the MTPA curve. Among them, the proposed IFOMFSMC tracks the MTPA curve more accurately than the others. Furthermore, the current ripples of the IFOMFSMC along the MTPA curve were smaller and smoother than those of the FOMFSMC and PI, indicating better control performance.

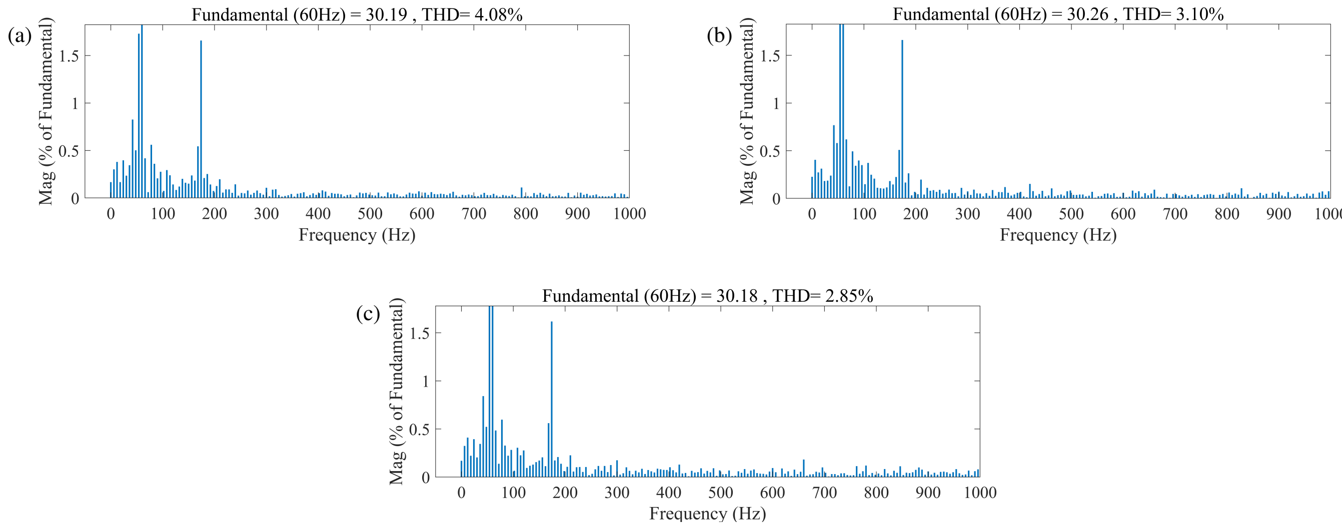

FIGURE 7. THD analysis of A-phase stator current. (a) THD analysis of A-phase stator current for PI, (b) THD analysis of A-phase stator current for FOMFSMC, and (c) THD analysis of A-phase stator current for IFOMFSMC.

Figures 6(e) and 6(f) present the comparison of the simulation results obtained using the ESMDO and FOESMDO under complex time-varying disturbance conditions. The results demonstrate that the performance advantages of the FOESMDO become more pronounced under complex time-varying disturbances acting on the system. Compared with the ESMDO, the FOESMDO's tracking accuracy showed a marked improvement, and the accuracy of disturbance estimation was effectively enhanced. In addition, the output signal of the FOESMDO exhibited good smoothness, and chattering was remarkably reduced.

Figure 7 presents the total harmonic distortion (THD) analysis of the A-phase stator current over ten current cycles starting from 1.35 s. The results indicate that, under the condition where only the speed loop is improved, the IFOMFSMC achieves the lowest THD, 2.85%. This benefit is attributed to the observer's more accurate real-time estimation and compensation of the unmodeled dynamics and disturbances in the system. Consequently, the THD of the IFOMFSMC was lower than that of the FOMFSMC, which is 3.10%, and that of the PI, which is 4.08%.

Table 6 lists the control performance indices of the three methods under complex time-varying disturbance conditions. Figure 8 shows the comparison of various performance indicators for the three control methods. It can be observed that all performance indicators of the IFOMFSMC were superior to those of the PI.

TABLE 6. Comparison of control performance indices.

Performance indicators	PI	FOMFSMC	IFOMFSMC
Speed response	0.375	0.261	0.159
Speed overshoot	3.3	60.5	0.09
Speed tracking error	0.535	0.095	0.063
Steady-state speed error	0.181	0.064	0.051
Torque ripple	1.95	1.79	1.38
i_aTHD	4.08%	3.10%	2.85%

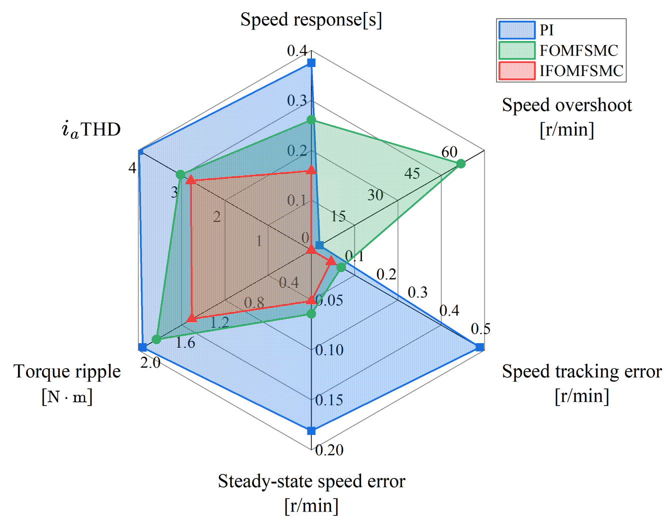

FIGURE 8. Comparison of control performance.

In summary, compared with single time-varying disturbances, the IFOMFSMC achieves more significant performance improvements in robustness, steady-state error reduction, and speed-tracking capability under complex time-varying disturbances. Therefore, as time-varying disturbances become more complex, the control performance advantage of the IFOMFSMC over the PI becomes more pronounced.

6. CONCLUSION

To address the issue of the actual speed not reaching the reference speed in a high-precision speed regulation system of the PMSM using a conventional MFSMC, an FOMFSMC method is designed in this study. By combining the FOSMC with the MFC, this method effectively improves speed response performance, achieves high-precision control of the PMSM, and solves dependence on an accurate mathematical model. Based on this, an IFOMFSMC method was further developed by introducing a new term, improving the reaching law, and incorporating the FOESMDO. This method further enhances the system's robustness and other performance indices under time-varying disturbances. The simulation results demonstrate that the proposed method enables the actual speed to track the reference speed accurately. Under a single time-varying disturbance condition, the performance of the IFOMFSMC is improved compared with that of the FOMFSMC and PI. Under complex time-varying disturbance conditions, the performance improvement of the IFOMFSMC is more significant; compared with PI, the speed response and tracking capability are improved by 57.6% and 88.2%, respectively, while the steady-state speed error and torque ripple are reduced by 71.8% and 29.2%. Under such operating conditions, the dynamic and steady-state performances as well as the robustness of the control system are effectively enhanced.

The following aspects of this study can be further investigated in the future. First, the computational complexity of the proposed method has not been fully considered. Future work can conduct an in-depth study on the computational complexity to ensure the feasibility of real-time implementation of the algorithm. Second, the current control method is mainly focused on operations below the base speed. Combining it with flux-weakening control to verify its performance in the high-speed deep flux-weakening region is crucial for expanding its application range. Third, the suppression effect of the THD still has room for improvement. Therefore, a coordinated control optimization method for the current loop can be designed in the future to optimize the overall performance of the current, voltage, and speed loops.

ACKNOWLEDGEMENT

This work was supported by the Natural Science Foundation of Hunan Province Number (2026JJ80067).

REFERENCES

[1] Tong, J., K. Zhao, Y. Chen, J. Cao, Y. Duan, and J. Xiong, "An improved equivalent-input-disturbance method based on enhanced estimators for wideband disturbance suppression in PMSM," *Progress In Electromagnetics Research C*, Vol. 165, 79–88, 2026.

[2] Zhang, X., C. Zhang, Z. Wang, and J. Rodríguez, "Motor-parameter-free model predictive current control for PMSM drives," *IEEE Transactions on Industrial Electronics*, Vol. 71, No. 6, 5443–5452, 2024.

[3] Guo, X., S. Huang, K. Lu, Y. Peng, H. Wang, and J. Yang, "A fast sliding mode speed controller for PMSM based on new compound reaching law with improved sliding mode observer," *IEEE Transactions on Transportation Electrification*, Vol. 9, No. 2, 2955–2968, 2023.

[4] Lin, F.-J., M.-S. Huang, C.-Y. Hung, and Y.-C. Chien, "Intelligent computed torque control with recurrent legendre fuzzy neural network for permanent-magnet assisted synchronous reluctance motor," *IEEE Access*, Vol. 11, 54 017–54 028, 2023.

[5] Chen, Z., A. A. Dawara, X. Zhang, H. Zhang, C. Liu, and G. Luo, "Adaptive sliding mode observer-based sensorless control for SPMSM employing a dual-PLL," *IEEE Transactions on Transportation Electrification*, Vol. 8, No. 1, 1267–1277, 2022.

[6] Rsetam, K., M. Al-Rawi, A. M. Al-Jumaily, and Z. Cao, "Finite time disturbance observer based on air conditioning system control scheme," *Energies*, Vol. 16, No. 14, 5337, 2023.

[7] Ali, K., Z. Cao, K. Rsetam, and Z. Man, "Robust adaptive integral fast sliding mode control for servo motors," *Mechatronics*, Vol. 117, 103504, 2026.

[8] Zhao, K., T. Yin, C. Zhang, X. Li, Y. Chen, and J. He, "Research on model-free sliding mode control of permanent magnet synchronous motor," *Journal of Electronic Measurement and Instrumentation*, Vol. 32, No. 4, 172–180, 2018.

[9] Zhao, K., W. K. Dai, R. R. Zhou, A. Leng, W. Liu, P. Qiu, G. Huang, and G. Wu, "Novel model-free sliding mode control of permanent magnet synchronous motor based on extended sliding mode disturbance observer," *Proceedings of the CSEE*, Vol. 42, No. 6, 2375–2386, 2022.

[10] Li, X., Y. Yang, Y. Zhou, W. Liu, and K. Zhao, "The non-singular fast terminal sliding mode control of interior permanent magnet synchronous motor based on deep flux weakening switching point tracking," *Energy Engineering: Journal of the Association of Energy Engineers*, Vol. 120, No. 2, 277–297, 2023.

[11] Li, X., J. Liu, K. Zhao, Y. Yin, and L. Zou, "Improved non-singular Fast terminal sensor-less sliding mode control of IPMSM considering external disturbance and parameter perturbation," *Progress In Electromagnetics Research B*, Vol. 102, 81–98, 2023.

[12] Feng, Y., F. Han, and X. Yu, "Chattering free full-order sliding-mode control," *Automatica*, Vol. 50, No. 4, 1310–1314, 2014.

[13] Borkar, A. and P. M. Patil, "Super twisting observer based full order sliding mode control," *International Journal of Dynamics and Control*, Vol. 9, No. 4, 1653–1659, 2021.

[14] Hou, H., X. Yu, L. Xu, K. Rsetam, and Z. Cao, "Finite-time continuous terminal sliding mode control of servo motor systems," *IEEE Transactions on Industrial Electronics*, Vol. 67, No. 7, 5647–5656, 2020.

[15] Wei, C., J. Xu, Q. Chen, C. Song, and W. Qiao, "Full-order sliding-mode current control of permanent magnet synchronous generator with disturbance rejection," *IEEE Journal of Emerging and Selected Topics in Industrial Electronics*, Vol. 4, No. 1, 128–136, 2023.

[16] Li, X., Z. Yi, J. Liu, K. Zhao, and L. Zou, "Deep flux weakening of IPMSM based on feedback super-twisting non-singular fast terminal sliding mode control," *Journal of Electronic Measurement and Instrumentation*, Vol. 38, No. 11, 132–145, 2025.

[17] Fang, X., L. M. Wang, and K. Zhang, "High order nonsingular fast terminal sliding mode control of permanent magnet linear motor based on disturbance observer," *Transactions of China Electrotechnical Society*, Vol. 38, No. 2, 409–421, 2023.

[18] Guo, X., S. Huang, Y. Peng, *et al.*, "Sliding mode control of IPMSM speed regulation system based on an improved double power reaching law and global fast terminal sliding mode observer," *Transactions of China Electrotechnical Society*, Vol. 38, No. 1, 190–203, 2023.